AIAA JOURNAL
Vol. 50, No. 3, March 2012

Rayleigh Scattering Density Measurements, Cluster Theory, and Nucleation Calculations at Mach 10

R. Jeffrey Balla* and Joel L. Everhart†
NASA Langley Research Center, Hampton, Virginia 23681

DOI: 10.2514/1.J051334

In an exploratory investigation, quantitative unclustered laser Rayleigh scattering measurements of density were performed in the air in the NASA Langley Research Center's 31 in. Mach 10 wind tunnel. A review of 20 previous years of data in supersonic and Mach 6 hypersonic flows is presented where clustered signals typically overwhelmed molecular signals. A review of nucleation theory and accompanying nucleation calculations are also provided to interpret the current observed lack of clustering. Data were acquired at a fixed stagnation temperature near 990 K at five stagnation pressures spanning 2.41 to 10.0 MPa (350 to 1454 psi) using a pulsed argon fluoride excimer laser and double-intensified charge-coupled device camera. Data averaged over 371 images and 210 pixels along a 36.7 mm line measured freestream densities that agree with computed isentropic-expansion densities to less than 2% and less than 6% at the highest and lowest densities, respectively. Cluster-free Mach 10 results are compared with previous clustered Mach 6 and condensation-free Mach 14 results. Evidence is presented indicating vibrationally excited oxygen and nitrogen molecules are absorbed as the clusters form, release their excess energy, and inhibit or possibly reverse the clustering process. Implications for delaying clustering and condensation onset in hypersonic and hypervelocity facilities are discussed.

I. Introduction

LASER Rayleigh scattering (LRS) has become an important research tool to study a variety of processes including fluid dynamics, combustion, and atmospheric science [1]. LRS elastically scatters photons in the laser beam off gas molecules in the flow. Scattered light occurs at the same wavelength as the laser. Scattered light is proportional to the sum of all species in the gas weighted by their respective Rayleigh cross sections. By calibrating under known species conditions, density is measured.

LRS has inherent advantages as an offbody molecular diagnostic in high-speed flows. Since no seeding is required, problems associated with particles or molecular seeds such as uniform seeding, particle lag, corrosion of facility, and toxicity are avoided. Unlike physical probes, LRS is nonintrusive. This is particularly important in the study of supersonic and hypersonic flows. Flowfield imaging with high spatial resolution is possible using a two-dimensional (2-D) detector. Line or planar measurements allow particles to be identified and rejected. LRS can quantify the freestream, postshock, and possibly the wake flow for computational fluid dynamics (CFD) code validation. It can also be used for facility calibration, flow quality measurements, quantitative line and planar density measurements in the flowfield around flight research vehicles, and visualization of structures enhanced by clustering or condensation.

The next section will briefly present the historical development of LRS. This will be followed in Sec. III by a discussion of the considerable development effort at the NASA Langley Research Center (LARC) in applying LRS for not only flow visualization but also line and planar measurements of density in subsonic, supersonic, hypersonic, and hypervelocity full-scale ground-test wind tunnels, where the test gas is typically air. These discussions provide the foundation for the subsequent experimental and theoretical analysis, results, and conclusions.

Received 11 April 2011; revision received 12 September 2011; accepted for publication 1 October 2011.

*Senior Research Scientist, Advanced Sensing and Optical Measurement Branch, Mail Stop 493; Adjunct Professor, Physics Department, Old Dominion University, Norfolk, Virginia 23529; robert.j.balla@nasa.gov. Senior Member AIAA.

†Senior Research Engineer, Aerothermodynamics Branch, Mail Stop 408A. Associate Fellow AIAA.

II. Historical Laser Rayleigh Scattering Studies

Many groups, including researchers at the LARC, have investigated the use of LRS for fluid dynamic studies. Early studies obtained 2-D and three-dimensional (3-D) images of molecular density in a turbulent subsonic propane jet using a continuous argon-ion laser [2] or a 15 ns single pulse from an Nd:YAG laser in Freon to enhance signal levels [3,4]. Later subsonic studies over model wing surfaces increased signal levels using ultraviolet excimer lasers [5]. Two-dimensional images were acquired in air in supersonic flows [6], at Mach 1.5 [7], at Mach 2.5 [8], and in hypersonic flow at Mach 6 [9–11]. Most attempts at density measurements were frustrated in supersonic and hypersonic flows by clusters or condensation that overwhelmed molecular LRS signals. Clustering is a precursor to either condensation/liquefaction for air or solidification for nitrogen or expansion into a supersaturated/supercooled state. Studies have used CO_2 clustering and condensation to aid 0.5 MHz imaging of shock-wave/boundary-layer interactions in a Mach 2.5 wind tunnel [12].

At cooling rates of 10^6 K/s encountered in hypersonic nozzles, molecules of air attain cryogenic temperatures and agglomerate, forming clusters that can grow in size along the nozzle and test section. Eventually, the LRS signal from these clusters exceeds the LRS signal from air molecules, preventing quantitative density measurements [9]. Condensation was encountered when supersonic and hypersonic tunnels were first constructed in the 1940s [13,14]; using dryers eliminated water condensation shocks. Air liquefaction and nitrogen solidification issues were resolved by constructing heaters around the stagnation chamber to maintain expanded flow at sufficiently high temperatures. At Mach numbers above 10, testing required inaccessible or impractical stagnation temperatures. This problem was overcome when a region of supersaturation was discovered where single-phase flow could still be maintained [15,16]. Pure nitrogen is often chosen as the test gas since it has the highest vapor pressure of any air constituent. However, foreign particles such as oxide dust from the heaters or silica gel from the dryers [13,14] can act as condensation nuclei, resulting in condensation before supersaturation is reached. This problem is reduced using particle filters. Because of financial constraints, most LARC facilities use air as the test gas. Unfortunately, constituents such as trace amounts of

water and naturally occurring carbon dioxide with lower vapor pressures can condense at higher temperatures than nitrogen or oxygen and act as heterogeneous condensation nuclei [13,16,17] for all air constituents. Although modern hypersonic wind tunnels employ all condensation prevention methods, clustering has been observed in all Mach 6 facilities at LARC [9–11].

III. Laser Rayleigh Scattering Studies at NASA Langley Research Center

LRS has been attempted in a wide variety of LARC facilities because of its potential advantages for density measurements. Successful quantitative density measurements were made using LRS along a line in the 0.3 m Transonic Cryogenic Tunnel with a near-backward scattering geometry using a continuous-wave Nd:YAG at 532 nm laser [18]. This is a subsonic–transonic facility that uses high pressures combined with cryogenic nitrogen as a test gas to achieve high Reynolds numbers. Freestream densities and temperatures ranged from 3×10^{19} to 24×10^{19} molecules/cm^3 and from 100–300 K, respectively. Attempts to acquire quantitative planar LRS density in a supersonic boundary layer using a pulsed 10 ns Nd:YAG laser at 532 nm were unsuccessful at Mach 2.5 in test section 2 in the Unitary Plan Wind Tunnel [19]. LRS signal levels were 500 times greater than calculated freestream values and were attributed to oil clusters.

Point LRS using a continuous-wave argon-ion laser at 514.5 nm has been successful in the hypervelocity 22 in. Mach 20 helium facility. Helium is considered a noncondensible gas [20]. Time-averaged freestream density measurements from 1.7–4.5 K showed good agreement with computed freestream values. Since helium can expand to temperatures as low as 1.7 K without liquefying at the corresponding freestream low pressures, it does not require heating of the stagnation chamber for Mach numbers less than 28 [21].

A combined 10 ns 532 nm Nd:YAG-laser-based Rayleigh and Raman instrument was used to study flow in the 20 in. Mach 6 facility (20M6) along a line [9]. This facility was operated at stagnation pressures from 0.41 to 3.27 MPa (60–475 psia) and stagnation temperatures from 483–519 K (410–475°F). The instrument provided simultaneous measurements of Rayleigh signal levels both in the freestream and in a model flowfield. It also provided measurements of rotational Raman scattering of molecular nitrogen in the freestream to measure rotational temperature and vibrational Raman scattering of molecular nitrogen or oxygen to measure freestream density. Rayleigh results indicated the presence of freestream clusters generated as a result of cooling, which takes place in the expansion process over essentially the entire facility-operating envelope. Cluster density was estimated at 2×10^6 molecules/cm^3. Since light scattering scales as cluster radius to the sixth power [22], a single cluster of 15 nm effective radius can produce Rayleigh signals on a single charge-coupled device (CCD) pixel that are approximately one order of magnitude greater than those produced by the total gas molecular number density (2×10^{18} molecules/cm^3) having 0.1 nm radius. Assuming homogeneous nucleation, oxygen was considered as a possible cause of clustering. Raman temperature and density results showed clusters have no measurable effect on bulk flow properties. Clusters decreased with increasing stagnation temperature and decreasing stagnation pressure.

An argon-fluoride (ArF) excimer laser at 193 nm was used for LRS in the Mach 6 high-Reynolds-number (HRN M6) facility [10]. This laser has advantages that increase signal levels and allow extension of measurements from a line to a plane. First, the Rayleigh scattering cross section in air at 193 nm is ~80 times stronger than that at 532 nm, resulting from an ω^4 frequency scaling combined with resonance enhancement from nearby electronic transitions [23,24]. Second, scattering from optical surfaces such as stainless steel is typically less than 30% at ultraviolet wavelengths, compared with greater than 60% for visible wavelengths [25]. Scattering from large particles is also reduced [5]. Hence, signal to noise is increased because background scatter is reduced, and Rayleigh scattering can be used near surfaces.

Under typical facility-operating conditions [$P_t = 6.9$ MPa, $T_t = 520$ K (1000 psia, 475°F)], the freestream density in the HRN M6 facility [10] is 5×10^{18} molecules/cm^3. The detection limit obtained showed that planar, quantitative density measurements could be made over a 5×10 cm area in this rarefied flowfield in the absence of clusters using 60 mJ of laser energy. For the experimental goals in the HRN M6 facility, stagnation conditions were set at $P_t = 4.12$ MPa and $T_t = 520$ K ($P_t = 600$ psi and $T_t = 476$°F). Clusters were observed in all freestream images at both stagnation conditions. Finally, qualitative agreement was observed between the averaged Rayleigh results and reduced mean-mass density obtained from probe measurements. This suggested that clusters were tracking the local density. Results showed that, by careful application of this technique, useful measurements of relative density (or density ratio) could be obtained in the presence of clusters.

In an attempt to generate a cluster-free freestream by increasing stagnation temperature, LRS was performed in the 15 in. Mach 6 (15M6) high-temperature tunnel in air using an ArF excimer laser [11]. This facility produces the maximum stagnation enthalpy currently known for any large-scale Mach 6 wind tunnel. It can achieve stagnation temperatures as high as 700 K (800°F) over a range of stagnation pressures from 0.35 to 2.07 MPa (50–300 psia). The freestream was cluster free at stagnation pressures from 0.35 to 1.75 MPa and clustered above this range. Density measurements were also obtained in the bow shock and wake of a 38.1-mm-diam cylindrical model. All measured densities were in good agreement with CFD predictions.

Since nucleation theory discussed in Sec. VII predicts clustering will increase exponentially with decreasing freestream temperature, there have been no attempts since 1995 to apply LRS for cluster-free density measurements in air at or above Mach 6. This paper presents measured freestream density results from a recent exploratory opportunity that expands the LRS wind-tunnel application database to a large-scale Mach 10 air wind tunnel. Surprisingly, cluster-free Rayleigh scattering was discovered over the full range of stagnation pressures at a stagnation temperature of 990 K (1325°F).

IV. Experimental Methods

LRS was performed in the LARC 31 in. Mach 10 (31M10) air tunnel. While most Mach 10 facilities are combustion heated, the 31M10 facility is a unique large-scale 12.5 MW electrically heated blowdown-mode facility [21]. The test gas is air that is dried using an activated alumina dryer, providing a dew point temperature of 232 K (−41°F) at a pressure of 4.14 MPa (600 psi). It passes sequentially through three inline filters (20, 10, and 5 μm) to remove particles. The first two filters are pleated cloth that are replaced yearly due to degradation. This procedure maintains the third sintered stainless steel 5 μm filter in nearly pristine condition, and it is seldom replaced. Pressure drop across the filters is continually monitored to assess degradation with time.

The tunnel top wall is 15-5 stainless steel, and the three remaining walls are 17-7 stainless steel. The settling chamber, nozzle throat, test section, second adjustable minimum, and subsonic diffuser are water-cooled. Gas is expanded using a 3-D contoured nozzle to generate a nominal Mach number of 10 in the test section. This nozzle design minimizes centerline disturbance characteristic of axisymmetric contoured nozzles, resulting in a highly uniform core flow [21]. The nozzle throat is 2.72 cm^2, and the test section is 78.7 cm^2. At low stagnation pressures, the core flow is 25% of the test section or ±10 cm about the centerline, increasing to ±15 cm as the tunnel wall boundary layer thins with increasing test pressure. Optical access is provided by three uncoated Corning 7980 windows with transmissions greater than 85% at 193 nm. Windows are approximately 17 in. wide and 2.16 in. thick, which form three orthogonal walls of the test section. Top, side, and bottom window lengths are 28, 31, and 44.5 in. long, respectively. Models are positioned on the facility centerline in less than 0.6 s using a hydraulically operated injection system mounted on the rear sidewall.

Facility test times are a maximum of 60 s using one 60-ft-diam and two 40-ft-diam vacuum spheres. A low-pressure preheat of the nozzle walls is performed before each run. Typically, as in this experiment, the facility operates at a stagnation reservoir temperature (T_t) of 1000 K (1350°F) to prevent air liquefaction, over a stagnation pressure (P_t) range from 2.41 to 10.0 MPa (350–1450 psia). Flow properties for the facility are typically determined using the GASPROPS code developed by Hollis [26]. However, for the present purpose, flow conditions were determined assuming an isentropic expansion.

Figure 1 presents a virtual diagnostics interface (VIDI) representation [27] showing all details of the 31M10 facility and the optical setup for LRS line measurements. VIDI is a LARC software tool for interactive 3-D display of the facility, test article, data, and CFD prediction. The exploratory nature of the experiment constrained facility setup time to two days and allowed only a single day for testing, dictating the use of an easy-to-transport rapid-setup light source. Based on these constraints combined with an initial expectation of freestream clustering, a low-pulse-energy Lambda Physik OpTexPro excimer laser was selected. The laser was operated in broadband mode on ArF near 193 nm at 30 Hz. The unpolarized output passes through approximately 1 m of air before it enters the facility. It is turned 90 deg with a mirror and focused 0.71 ms downstream from the nozzle exit along a line normal to the flow near the center of the facility using an uncoated 600 mm focal length Suprasil lens. The Rayleigh scattered signal generated along a 36.7 mm line in the freestream is imaged using a gated double-intensified ITT Corporation model F4577 CCD camera. The detector has 240 vertical (27 μm) and 754 horizontal (11.5 μm) pixels and 15% quantum efficiency at 193 nm. The imaging system has been described [10]. The resulting RS170 video signal is digitized at 30 frames per second using an EPIX model PIXCI SV5 frame grabber card and stored in a computer. The frame grabber was modified to output a field index pulse at 30 Hz for synchronizing the laser, CCD camera gate, and frame grabber card. The computer can acquire 371 images (64 MB of memory) during a 12.4 s time interval. Six seconds are required to store the data. For this freestream data set, one single series of 371 images was acquired at each stagnation condition.

The excimer laser was operated in high-voltage constant mode. The manufacturer's specified shot-to-shot variation in laser energy is less than 3%. Laser output slowly decreases during each day as fluorine is consumed. To maintain constant energy during calibration and facility runs, laser high voltage is set to produce 5 mJ per pulse, half the maximum output. The typical initial high-voltage setting is 20% of full scale. Output energy is reduced by a factor of 2 due to transmission losses. Half of what remains has the correct polarization. Hence, experiments were performed using 1.25 mJ focused inside the test section. Constant laser energy is maintained by slowly increasing high voltage during the day from typically 20 to 40% of full scale. The laser is equipped with an internal energy monitor that displays the current pulse energy in real time using software. This output was monitored visually as a function of time. During any given data set, energy decrease was less than 5%. Ambient stray light was minimized using a 5 μs intensifier gate and by extinguishing the room lights. Laser timing jitter was $\pm$100 ns.

In previous 15M6 and HRN M6 Rayleigh experiments, extensive optical baffling was used to reduce laser light scattered from windows and walls. The use of optical baffles in the 31M10 and the 20M6 was prevented by wind-tunnel operational constraints. Accordingly, after averaging over 371 images, scattered laser light in the freestream at each pixel constituted 74% of the total signal (Rayleigh plus scattered light signal) at the lowest stagnation pressure and 16% at the highest pressure.

The calibration procedure for each pixel along the laser line has been described in [9]. Briefly, the facility was evacuated to prescribed pressures over the range of interest, and Rayleigh data were acquired. Calibration pressures were converted to calibration densities using stable wall temperatures obtained from a thermocouple in contact with the sidewall of the facility. LRS signals were obtained by averaging 371 images at each calibration density. A linear plot of the Rayleigh signal as a function of the air density was obtained for each of the 240 pixels along the 36.7 mm imaged line. Using a linear least-squares fitting routine, the slope and intercept, and their associated uncertainties, were calculated and stored in a file. The flowfield signals were converted to density using this calibration file. This procedure removed the systematic nonuniformities in the laser-camera system. The 31M10 facility was significantly cleaner than all three previous Mach 6 facilities studied. No large particles and few small particles were encountered during the calibration process or during Mach 10 operation. Typically, one small particle or fewer was observed for any given pixel along the imaged line every 371 images. Each particle increased signal by a maximum of $\sim$30%. Since particle influence on the average data was negligible, no attempts were made to remove these signatures from the data analysis. Applying the calibration to static facility data yielded results similar to those discussed previously in [9].

V. Mach 10 Rayleigh Density Measurement Results

Figure 2 shows the first LRS freestream density measurements in a Mach 10 air wind tunnel along a 36.7 mm line. Stagnation temperatures were 990 $\pm$ 11 K during all runs. Each line is the average over 371 images at stagnation pressures of 2.41, 4.49, 6.22, 8.64, and 10.0 MPa (corresponding to 350, 651, 902, 1254, and 1454 psi, respectively) with 1% variation during the run. Signals spanned 210 of 240 CCD pixels due to signal dropoff near both edges of the detector.

Figure 2 line traces are in good agreement with expected freestream density at all stagnation pressures. Based on previous clustered Mach 6 results, signal levels at least 10 times larger were expected due to freestream clustering. Figure 2 shows no evidence of clustering at any test pressure. Unfortunately, because of the exploratory nature of the experiment, they were acquired using low

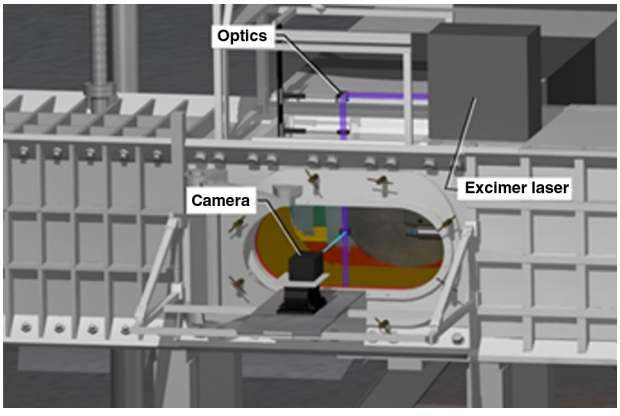

Fig. 1 VIDI representation of the 31M10 wind-tunnel test section and ultraviolet LRS setup.

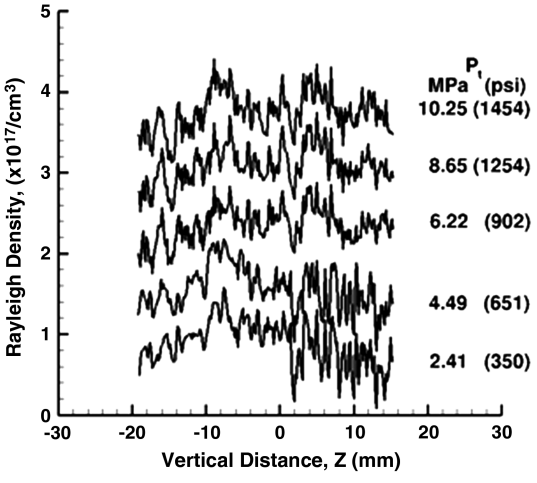

Fig. 2 Measured average freestream density.

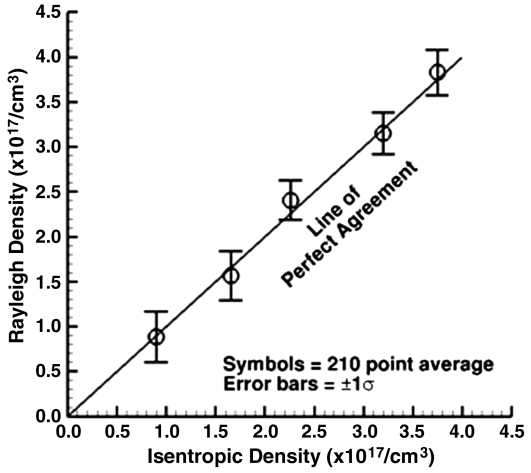

Fig. 3 Average measured freestream Rayleigh density versus computed density using isentropic expansion.

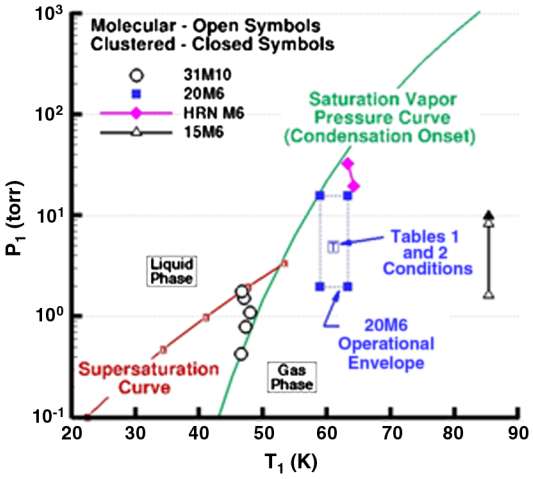

Fig. 4 Gas-liquid phase diagram and condensation onset for air compared with LRS measurements showing clustered and molecular results.

laser energies without optical baffles. At 2.41 MPa, signals were only one order of magnitude above the detection limit. To compensate, results are heavily averaged in time and space. Still, results show relatively flat density profiles with standard deviations averaging $0.252 \times 10^{17}/\text{cm}^3$ yielding percent of measurement values ranging from 32 to 6% at the lowest and highest freestream densities, respectively. These are upper limits to the flowfield spatial nonuniformity.

It was expected that the 3-D contoured Mach 10 nozzle would prevent centerline disturbances characteristic of axisymmetric contoured nozzles and produce a highly uniform core flow. In general, this is verified by the freestream density variation. However, Fig. 2 line plots show a consistent density dip near the 1 mm position for all test pressures. Although this is within the spatial calibration uncertainty for the facility centerline, its intensity weakens and broadens slightly with increasing freestream density. This disturbance will be explored with higher laser energy in a future entry, providing an increased signal-to-noise ratio. For reference, the spatial resolution of the LRS apparatus is ~0.48 mm (3 pixels) compared with 3.2 mm of typical pitot tube rakes.

Figure 3 shows the average measured density using 371 images and standard deviations (spatial rms) of the mean density based on 210 measured average densities along each line in Fig. 2 plotted against their respective densities computed using isentropic expansion. This is the uncertainty in the mean of the data from a single line. The solid line of perfect agreement between theory and experiment is drawn with a slope of one and an intercept of zero. Results show less than 2% disagreement between experimental and isentropic-expansion values at the highest densities and less than 6% at the lower densities. Results show no evidence of clustering over the entire operating stagnation pressure range of the facility at an average stagnation temperature of 990 K.

VI. Comparison of Rayleigh Density Measurements with Air–Liquid-Vapor Pressure Curve

The liquid-gas-phase diagram for air is shown in Fig. 4. As taken from Furukawa and McCoskey [28], the saturation vapor pressure curve is calculated using

$$\ell_n P(\text{torr}) = 16.6045 - 810.767/(T(\text{K}))$$

The line with open squares indicates the location of empirically measured condensation onset measured by Daum [15]. His data, represented by the small open squares, are well fit from 14–53 K using

$$\ell_n P(\text{torr}) = -8.7109 + 1.3579^* T^{0.5}$$

Freestream density and temperature conditions are plotted showing locations of molecular (open symbols) and clustered (filled symbols) LRS signals in the 15M6 (triangles), 20M6 (squares), HRN M6 (diamonds), and 31M10 (circles). Since clustered LRS signals were realized in 20M6 under all conditions, only four points representing the operational limits of the facility are plotted. The square-T symbol located inside the 20M6 operational limits indicates conditions used in calculations presented in Tables 1 and 2. It indicates the predicted conservative location where the total LRS signal is composed of equal amounts of molecular and clustered components [9]. Although all vapor pressures in 20M6 and HRN M6 facilities are below the saturation vapor pressure curve, LRS signals show clustered results. The 15M6 results acquired at the maximum facility stagnation temperature of 700 K have molecular LRS signals at stagnation pressures from 0.35–1.75 MPa (50–254 psi), and they transition to clustered LRS signals at 2.41 MPa (350 psi). For 15M6 at 85 K, the LRS are consistent with molecular densities when air vapor pressure is 140 times below the saturation vapor pressure curve. For 20M6 at 63 K, extrapolation of clustered results suggested molecular densities at 1 torr or 50 times below the saturation vapor pressure curve. For Mach 6 facilities under these conditions, these are good rules of thumb when considering LRS for quantitative density measurements. In stark contrast with all Mach 6 results are the 31M10 results. While vapor pressures start in the gaseous state, cross the saturation vapor pressure curve, span the supersaturated state, and intersect the supersaturation curve, all 31M10 LRS signals are consistent with molecular Rayleigh scattering. Next presented is Sec. VII, providing a brief tutorial of nucleation theory that lays the foundation for a discussion of these results in Sec. VIII.

VII. Homogeneous Nucleation Theory and Calculations

This section provides a brief tutorial and relevant equations concerning nucleation theory. For homogeneous gas-phase nucleation, cluster formation begins as a collision between two similar molecules. Clusters change size by attachment or loss of a single molecule as follows:

$$A_n + A_1 <--> A_{(n+1)} + \text{heat} \tag{1}$$

There must be sufficient collisions with the surrounding vapor to remove this energy or no further growth of the cluster will occur. This heat release to the surrounding vapor by collisions is the driving mechanism behind cluster formation. Under supersaturation conditions, the cluster grows to droplet size, and eventually condensation occurs.

The nucleation rate [29] in units of clusters of n molecules/$\text{cm}^3 \cdot \text{s}$ is given by

$$J = Z\beta O^* C_0 \exp((-\Delta G^*)/kT) \tag{2}$$

Table 1 Characteristics of the 20M6 and 31M10 air wind tunnels relevant to cluster formation

Facility	20M6	31M10	Units
Stagnation parameters			
Pressure	1.03	10	MPa
	150	1450	psi
Temperature	505	990	Kelvin
	450	1349	Fahrenheit
Nozzle length throat to exit	2.27	4.817	meters
Nozzle type	2-D contoured	3-D contoured	
Particle filters	10	20, 10, and 5	micrometers
Freestream parameters			
Mach number	6	10	
Static density	7.9	3.6	$\times 10^{17}$ molecules/cm^3
Static pressure	0.612	0.225	kPa
	4.9	1.8	torr
Static temperature	61.6	47.9	Kelvins
Velocity	949	1394	m/s
Collision frequency	7.4	3	$\times 10^7$ collisions/s
Test section parameters			
Nozzle exit to measurement location length	3.08	0.71	meters
Residence time	3.25	0.51	msec
Total N_2-N_2 collisions	19	1.2	$\times 10^4$ collisions
Cluster parameters			
Detectable cluster density	2	1	$\times 10^6$ molecules/cm^3
Cluster radius	15	15	nanometers
Critical size	20	22	
N_2 nucleation rate[a]	4.6	100	$\times 10^{-14}$ clusters/cm^3-s
N_2 relaxation time	14	5	$\times 10^{-8}$ s
N_2 relaxation collisions	4	4	collisions
Energy			
Total $V'' = 1$ population[a]	11	197	$\times 10^{-21}$ J
N_2 $\Delta G(n = 100, T, p)$[a]	291	197	$\times 10^{-21}$ J

[a]Noteworthy nucleation calculations.

where $Z^2 = (\Delta G^*/kT)/[3\pi(n^*)^2]$ is the Zeldovich factor, $\beta = (p/2\pi mkT)^{1/2}$ is the rate at which molecules of mass m impinge on unit surface at states p and T, $O^* = (36\pi v^2)^{1/3}(n^*)^{2/3}$ is the cluster surface area with v as the molecular volume, C_0 is the gas-phase molecular number density, and $-\Delta G^*/kT$ is the critical Gibbs free energy of formation of a critical-size cluster containing n^* molecules at temperature T. A critical-sizes cluster is one where addition of one molecule will cause it to grow and loss of one will cause it to disappear.

$\Delta G(n, T)$ at any pressure is calculated using

$$\Delta G = \Delta G^0 + (1 - n)kT\,\ell_n(p/p^0) \tag{3}$$

Relaxation times required to remove the cluster energy and achieve steady state during nucleation in these rapid expansions is given by

$$1/\tau = 6.4Z^2\beta O^* \tag{4}$$

The number of relaxation collisions is obtained by multiplying the relaxation time by the freestream collision frequency.

Homogeneous nucleation calculations in both 20M6 and 31M10 are presented in Tables 1 and 2. The selected 20M6 stagnation conditions produce Rayleigh signals that are conservatively twice the molecular level, indicating the onset of detectable clustering (see Fig. 8 in [10]). Since these equations predict nucleation increases with increasing density, maximum clustering in 31M10 should be observed at the maximum stagnation pressure of 10 MPa (1450 psi). Calculations are performed for nitrogen since standard Gibbs free energy of formation values of n-meric clusters as a function of temperature (i.e., $\Delta G(n, T, P_o)$) are available [30]. No data are available for air or oxygen.

Although 31M10 density is reduced by a factor of 2.2 while temperature is 13.7 K lower than 20M6 conditions, nucleation calculations shown in Tables 1 and 2 predict $J_{31M10} = 22J_{20M6}$. This shows that the exponential temperature term dominates the linear density terms and even small temperature reductions can greatly increase nucleation. Unfortunately, the 31M10 test gas is air, not nitrogen. However, since both facilities share a common air supply, similar cluster compositions, mechanisms, and Gibbs free energies are expected, and these simplistic calculations should be indicative of relative facility trends. Whether the actual clustering mechanism is homogeneous nucleation or the mechanisms described below, the trends predicted by these calculations are assumed to be generally applicable. Therefore, higher nucleation rates are expected in 31M10 versus 15M6.

Table 2 Vibrational excitation parameters

		Boltzmann populations	
Species	Level (energy)	20M6	31M10
N_2	$V'' = 1$ (2330 cm^{-1})	0.0013	0.0355
	$V'' = 2$ (4631 cm^{-1})	0.0000019	0.00132
O_2	$V'' = 1$ (1556 cm^{-1})	0.0119	0.108
	$V'' = 2$ (3088 cm^{-1})	0.00015	0.012
	$V'' = 3$ (4595 cm^{-1})	0.0000021	0.00139
Total excited state $N_2 + O_2$ *population per 100 molecules*			
	$V'' = 1$	0.35	5.07
	$V'' = 2$	<0.0032	0.36

VIII. Discussion

No published data are available on clustering or condensation onset in the 31M10 facility. The assumption based on air condensation curves and experimental evidence based on pitot tube measurements was that condensation would be observed in the supercooled region at or above 8.6 MPa (1250 psi). Before Fig. 2 results, freestream clustering or condensation was expected in the 31M10 for three reasons. First, clustering was observed in the 20M6 and 15M6 facilities when air vapor pressures were 50–140 times below the computed air liquid-vapor phase diagram pressure curve. Figure 4 shows the 31M10 freestream vapor pressures cross this curve, span the supersaturation region, and overlap the condensation curve. Second, conditions for the observed onset of nucleation in 20M6 were compared with conditions under the maximum

freestream pressure in 31M10. Homogeneous nucleation calculations in Tables 1 and 2 predict 22 times greater rates in 31M10. Third, using Tables 1 and 2, the detectable-cluster threshold was two times lower in 20M6 than in 31M10, i.e., the ratio of molecular freestream densities. Surprisingly, results in Figs. 2 and 3 showed no clustering over the full range of 31M10 stagnation pressures. The discussion below begins with possible mechanisms that can create clustering and concludes with mechanisms that can prevent or destroy clustering.

The nucleation literature provides three possible mechanisms for cluster formation. The first is homogeneous nucleation of a single gas-phase species producing a cluster composed of identical atoms or molecules. This process occurs by spontaneous random cluster formation and requires significant vapor supersaturation [31]. Figure 4 shows supersaturation exists in 31M10. Although clustering was expected, signals are molecular. Figure 4 also shows 20M6 and 15M6 are clustered when vapor pressures are within two orders of magnitude of the saturation vapor pressure. Tables 1 and 2 nitrogen nucleation calculations for 31M10 and 20M6 were too slow for homogeneous cluster formation. In 20M6, this process was discounted for all air constituents except oxygen [9]. In supersonic flow experiments where cluster sizes have been measured, clusters were limited to less than 10 nm, and calculations in pure nitrogen or argon in supersonic flow supported this conclusion [32]. No air data is available. Clusters of typically 15 nm are required to account for 20M6 signals. The conclusion is that clusters in 20M6 and 15M6 are not caused by homogeneous nucleation of a single gas-phase species.

The second mechanism is heterogeneous nucleation in a multicomponent gas mixture [33]. This process starts on a molecular cluster generated from homogeneous nucleation of a single species as described in the first mechanism. The species with the lowest vapor pressure condenses first. Since the current flows contain 8×10^{12} molecules/cm^3 of water vapor [9], ice crystals are a possibility. Gases such as carbon dioxide, oxygen, argon, and nitrogen would follow [13,16,17]. Since the cluster is composed of several species, surface energy and the free energy barrier for formation of the cluster are lower. According to [32], only saturation vapor pressure, and not supersaturation, is required compared with homogeneous nucleation in the first mechanism. The result is increased nucleation rate compared with single species homogeneous nucleation. Calculations in a supersonic expansion predict an order-of-magnitude increase in particle mass and 10–200 nm final particle diameter [32]. Since 15 nm particles are required to account for 20M6 signals, this mechanism is a possibility.

The third mechanism is heterogeneous nucleation on preexisting particles or other solid or liquid substances in a multicomponent gas mixture [33,34]. These particles could be nanometer-sized particulates such as dust from poor facility hygiene or, specifically, heater oxide dust [13,14] or molecules, or droplets of compressor oil [19]. None of these can be removed by 5 μm filters. To produce the spatially uniform clustering observed in previous Rayleigh images, particles densities near 1×10^6 particles/cm^3 are required [9]. Typical atmospheric air and polluted air have densities of 100 to 1000 particles/cm^3, respectively. Since particles or aerosols already exist as nucleating agents, no delay time is required to form nucleating sites by spontaneous cluster formation from homogeneous nucleation. Hence, this mechanism can start earlier in the nozzle expansion than the above mechanisms. Clusters formed around particles are usually bigger than the critical radius. Time lags associated with growth to and beyond the critical radius are eliminated. The effective surface energy of the cluster is lower, and this reduces the free energy barrier for formation. In the first two mechanisms, saturation or supersaturation was required. In this mechanism, neither is required. The result is either faster cluster formation under comparable homogeneous nucleation conditions or comparable cluster formation at lower vapor pressures and higher temperatures. Cluster growth is accomplished by addition of gas components in air starting with water vapor and proceeding in the order described in the second mechanism.

All three mechanisms are complex and poorly understood, and data in air are essentially nonexistent. No instrumentation exists to detect in situ cluster composition, cluster distribution, or growth mechanisms. LRS can estimate cluster diameter once the cluster signal exceeds the molecular signal. The third mechanism (i.e., heterogeneous nucleation on preexisting particles in a multicomponent mixture) is consistent with all experimental observations in Fig. 4. Furthermore, it is consistent with the nucleation calculations in the 20M6 and 31M10 facilities, the literature calculations, and the literature experiments. The third mechanism is believed active in all Mach 6 facilities and 31M10. For the Mach 6 facilities, there are insufficient data to discount the second mechanism. Based on previous clustered results in Mach 6 facilities, clustering by homogeneous nucleation was expected in 31M10. Only the low nucleation rate calculation suggests it may not be active.

Since all facilities share the same air supply, there are few differences to explain the lack of clustering in 31M10. The 20M6 facility has a single 10 μm) fiberglass air filter, while the 31M10 has a series of three filters (20, 10, and 5 μm). Since a filter of 5 μm or greater cannot affect any of the nucleation mechanisms, this difference cannot be responsible for the observed results. Since no large particle interference is observed in the Rayleigh signals in the 31M10, the series of filters provide a much cleaner flow. The 3-D 31M10 contoured nozzle design creates a more gentle expansion compared with the more abrupt fixed-geometry 2-D Mach 6 contoured nozzle. In the latter case, the top and bottom walls are contoured, while the side walls are parallel. On a relative basis, this will inhibit clustering. However, it is unlikely that the 31M10 contoured nozzle design could prevent clustering at lower temperatures, at 100 times higher vapor pressures under supersaturation conditions, and at the condensation onset curve.

The only other differences between the 31M10 and 20M6 facilities are the stagnation and freestream conditions. Since lower freestream temperatures and supersaturation in 31M10 favor clustering, differences in the stagnation conditions are further examined. One consequence of the higher stagnation enthalpy in 31M10 is the production of a significant Boltzmann population of vibrationally excited states of nitrogen and oxygen (Table 2). These states have several notable characteristics. First, they contain significant excess energy. Second, due to their chemical nonreactivity and long lifetimes, vibrational Boltzmann populations persist unchanged or frozen through the nozzle expansion and along the full length of the test section [35]. Third, since clustering is a reversible process and Eq. (1) indicates heat addition can destroy a cluster, the vibrationally excited states of nitrogen and oxygen can transfer sufficient energy to the cluster to destroy it during every step of its growth process at all locations from the nozzle throat to the end of the test section. Previous researchers studying condensation in the Arnold Engineering Development Center Tunnel 9 (AEDC T9) nitrogen facility using Mach 10, 14, and 18 nozzles speculated "particle nucleation and growth might be strongly affected by release of this internal energy" [36]. The following paragraph presents evidence that this mechanism is responsible for the lack of clustering in 31M10.

Consider a 100-molecule cluster of air and a stagnation temperature of 990 K for 31M10, Tables 1 and 2 show that three molecules of $V'' = 1$ (first vibrationally excited ground state) nitrogen and two molecules of $V'' = 1$ oxygen statistically become part of the cluster assuming a simplistic single-molecule addition process during its formation. At 990 K, the contribution from $V'' > 1$ for nitrogen and oxygen is treated as negligible. The last two lines in Table 1 show that the Gibbs free energy of a nitrogen cluster under freestream conditions is comparable with the summed vibrational energy from these five molecules. This is true at 31M10 conditions but not 20M6 conditions. There is sufficient energy in the absorbed $V'' = 1$ molecules to inhibit and possibly reverse the condensation process by evaporating a large fraction of molecules in the cluster. Since air is 79% nitrogen, clusters in air are assumed to have Gibbs free energies similar to those in nitrogen. Hence, this argument should be applicable to a cluster formed in air independent of its composition or growth mechanism.

Tables 1 and 2 show that four collisions with gas-phase molecules are required to remove the excess single-molecule cluster energy during the relaxation time. For a 100 molecule cluster, this means

~400 collisions. Additional energy can be transferred from $V'' = 1$ to the cluster during these collisions. No data are available on the effectiveness of this transfer.

The nucleation process for the first two mechanisms exhibits an induction time required to form nuclei of a critical size. For air under 31M10 conditions, neither the length of the induction time nor the number of collisions involved is known. However, additional energy can be transferred to the cluster during this time by collision and absorption of $V'' = 1$ molecules. Since this is the slow step in the nucleation process, energy transfer during this critical time may be the dominant mechanism that prevents cluster growth. If the third clustering mechanism described above were active, this mechanism would not apply. In the absence of any data on energy transfer during the relaxation time and induction time of cluster formation, they are only noted as possibilities for the dominant mechanism of cluster destruction.

The conclusion is that LRS signals in 20M6 can be explained by clusters that are formed by heterogeneous nucleation on preexisting particles, or other solid or liquid substances in a multicomponent gas mixture, and then they begin to grow. There is insufficient vibrational population at 500 K stagnation temperature to prevent their growth. At an ~15 nm size radius, LRS signals from cluster densities estimated at 1×10^6 molecules/cm^3 would exceed those from purely molecular sources.

The third nucleation mechanism is believed to start early in the nozzle expansion in 31M10. During the nozzle expansion, the vibrational Boltzmann population of oxygen plus nitrogen will be a constant 5% of the density. At 10.25 MPa (1450 psi) stagnation pressure and 990 K, freestream total $V'' = 1$ is estimated at 1.8×10^{16} molecules/cm^3. Assuming each 100 molecule cluster consumes five $V'' = 1$ molecules, this process prevents clusters in 31M10 from growing to a size, which can dominate molecular LRS signals. At cluster densities of 1×10^6 molecules/cm^3 and nucleation rates where each cluster consumes five $V'' = 1$ molecules, this process would not measurably affect the freestream vibrational Boltzmann population. At high nucleation rates, this process would prevent observable clustering until most $V'' = 1$ are consumed followed by observation of clustered LRS signals, and eventually condensation. Regardless of the nucleation mechanism or cluster composition, they can all be destroyed by the $V'' = 1$ population.

Chemically reactive species are also created by the higher 31M10 stagnation enthalpy, such as oxides of nitrogen (NO, NO_2, and N_xO_y) or ozone produced in the heater by thermal equilibration or heterogeneous decomposition of air on hot surfaces of the heater elements. It is unlikely that cluster formation could be prevented by heat release from chemical reaction between clusters and these species. Even if present at parts-per-million levels by thermal equilibrium, collisions between clusters and $V'' = 1$ species should be at least 1000 times greater than between clusters and chemically reactive species. It is unlikely that a few molecules of the fully oxidized forms of these species could enter the cluster and significantly decrease the nucleation rate. However, early in the cluster formation, where water condensation could dominate, the reaction between water and NO_2 could produce one molecule of acid such as HNO_2 or HNO_3. One interesting, albeit unlikely, speculation is that this could change the pH of a 100-molecule cluster and inhibit clustering.

Several nitrogen data sets in the AEDC T9 facility support the $V'' = 1$ mechanism. Most compelling are those of Marren and Lafferty [37], who varied stagnation temperatures from 866–1605 K (19–53 K static temperature) while maintaining a constant stagnation pressure of 137.9 MPa (20,000 psi) at Mach 14. Experiments used laser light scattering from a 3 mW HeNe laser to detect condensation, not clustering. Freestream results for two data sets are reproduced in Fig. 5. The filled circle shows the only condition to exhibit condensation. Compared with 31M10 stagnation conditions of 1450 psi, AEDC T9 was operated at 20,000 psi stagnation pressure. Nucleation theory indicates the increased pressure should favor condensation. Still, as stagnation temperature was decreased from 1605 to 866 K (52–18 K static temperature), condensation-free flow was observed for all but the lowest stagnation temperature.

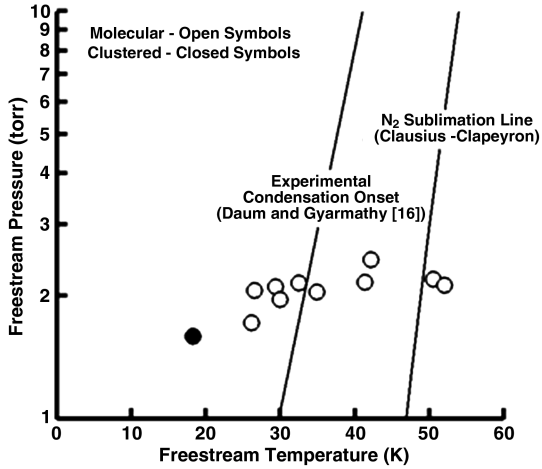

Fig. 5 Demonstration of significant freestream supercooling in N_2 beyond the condensation onset limit in the AEDC T9 wind tunnel (taken from [37]).

Freestream results from Lederer et al. [38] in AEDC T9 at Mach 14 and from Dolgushev et al. [39] at Mach 22 also showed condensation-free flow beyond the experimental condensation limit of Daum and Gyarmathy [16]. Griffith et al. [36] in AEDC T9 at Mach 14 studied condensation behind the shock on a sharp cone. Stagnation temperatures spanned 676–1839 K, and stagnation pressures spanned 32.8–142.76 MPa (4763–20,712 psi). Under all conditions presented, condensation was not observed until stagnation temperature dropped below 656 K.

All three AEDC T9 data sets indicate that condensation-free flow is achievable beyond the nitrogen condensation onset curve of Daum and Gyarmathy [16]. One possible explanation is the presence of $V'' = 1$. This region is difficult to map in air and nitrogen since few facilities can generate the required stagnation temperatures and pressures. Previous results suggest the theoretical limit of condensation would be 60% of the spinodal [36].

Of additional interest is the effect of vibrational levels above $V'' = 1$. With their increased energy, they may be more effective in preventing cluster formation. Tables 1 and 2 indicates their population is negligible at 990 K. Above 990 K, calculations suggest that, as a flow expands through the nozzle throat, temperatures and pressures are sufficiently high such that vibrational equilibration will occur until expansion temperatures reach 1000 K [36]. If true, natural effects of levels $V'' > 1$ are probably negligible. Future experiments are recommended to artificially introduce $V'' > 1$ and attempt to determine its effects on clustering.

It was noted that both the N_2 and O_2 molecules may experience anharmonic V-V transfer, resulting in vibrational distribution functions that are highly nonequilibrium. While the total number of vibrational quanta will indeed be approximately equal to that corresponding to a frozen vibrational temperature, the distribution could be much different, with molecules in $V'' = 1$ transferred to higher V'' levels [40].

LRS signals in 15M6 at 700 K stagnation temperature transition from molecular to clustered levels as stagnation pressure increases from 0.345–2.07 MPa (50–300 psi). No nucleation calculations were performed since freestream temperature is $\frac{2}{3}$ of the well temperature of the interaction potential and existing theory is likely invalid [30]. Assuming this is the temperature for $V'' = 1$ mechanism onset, its effect at this temperature will be weak. The lack of clustering is attributed more to reduced nucleation rates at 85 K than to the $V'' = 1$ mechanism. If operative, transition from molecular to clustered LRS signals near 2.07 MPa provides an estimate of the rate of $V'' = 1$ mechanism compared with the nucleation rate.

At stagnation temperatures of 700 K, a cluster of 100 molecules would collide with 0.66 $V'' = 1$ N_2 and 0.82 $V'' = 1$ O_2 molecules during its formation. This suggests the $V'' = 1$ mechanism will become active near 700 K. Consider the results in Fig. 4. Molecular

signal levels occur in 31M10 at 990 K; clustered signal levels occur below 700 K in both 20M6 and HRN M6. No clustering occurs in 15M6 near 700 K except at the highest stagnation pressure, but the effect is likely weak. One AEDC T9 data set shows condensation-free results from 676–1839 K and condensation at temperatures below 656 K. A second AEDC T9 data set shows condensation at 866 K and condensation-free results from 1116–1605 K. All data are consistent with $V'' = 1$ mechanism onset of 750 ± 100 K.

The implications of the $V'' = 1$ mechanism suggest future 31M10 experiments. Stagnation pressure should be systematically increased at a 1000 K stagnation temperature. The resulting increase in nucleation rates should provide a method for converting trapped vibrational energy into translational energy. This trapped energy has long been of concern to the hypersonic community. Benefits include improved accuracy of freestream parameters predicted by isentropic-expansion calculations, improved flow quality, and reduced complexity in modeling the flow over models. As stagnation pressure is increased, it may be possible to fine-tune the amount of vibrational nonequilibrium. This could be important for CFD calibration and fundamental flow physics studies. It should be possible to find the condition where most or all trapped vibrational energy is removed and clusters are prevented from growing to sufficient size to affect molecular Rayleigh scattering signals. Perhaps an increased facility operational envelope will emerge with improved flow quality and where Rayleigh scattering can be applied for quantitative density measurements. Further increases in stagnation pressure should provide a means of detecting the degree of supersaturation that can be achieved before condensation onset. There is insufficient energy in the nonequilibrium population compared with condensation energy to prevent condensation. However, it is possible that the $V'' = 1$ mechanism can delay condensation onset by energy transfer due to $V'' = 1$ absorption, collisional energy transfer during the cluster relaxation time, or by slowing the kinetics of the process by preventing formation of the critical cluster. Regrettably, these experiments require conditions that exceed the design limitations of the 31M10 facility.

Operationally, the maximum T_t in the 31M10 is 1061 K (1450°F), a constraint dictated by facility design limitations. Procedurally, the facility typically operates at $T_t = 1005$ K (1350°F), a constraint dictated by the desire to avoid condensation that is implemented in the flow calibration envelope. A desired experiment, then, is to combine LRS (density and clustering onset) with pitot pressure rake (pressure and condensation onset) measurements at offnominal stagnation temperatures from 600 to 1000 K in 50 K increments. Testing with the pitot pressure rake will allow examination of potential measurement differences as shown by the rake-cone differences in [36]. By varying stagnation pressure at each temperature, a larger operational envelope may emerge. Decreasing the T_t should result in reduced facility cost through energy reduction and heater stress. More important, decreasing the T_t also increases the accessible Mach-Reynolds numbers with good flow quality that is free from clusters and condensation. It may also provide air data to support condensation-free facility operation similar to AEDC T9 nitrogen test conditions beyond the condensation onset curves of Daum and Gyarmathy [16].

IX. Conclusions

In an exploratory experiment, the first quantitative cluster-free LRS measurements of freestream density have been demonstrated along a 36.7 mm line in a full-scale Mach 10 air wind-tunnel establishing technique viability. Experimental densities agree with isentropic-expansion calculations over the entire stagnation pressure range at 990 K. This is in contrast to 20 years of results in nearly all supersonic and hypersonic air flows where clustered signals typically overwhelm molecular signals. Quantitative density measurements have been demonstrated under supersaturation flow conditions using LRS. Lack of clustering and condensation is explained by a frozen vibrational nonequilibrium Boltzmann population of N_2 and O_2 molecules. They are created in the stagnation chamber and persist along the nozzle expansion and the full length of the test section. By combining nucleation and vibrational Boltzmann distribution calculations with previous Mach 6 clustered results, current cluster-free Mach 10 results, and previous nitrogen AEDC T9 results, the first evidence has been provided to confirm two-decades-old literature speculation [36] that vibrational energy transfer from the nonequilibrium Boltzmann population to a cluster can reduce or prevent cluster formation and growth. Data from five facilities are consistent with $V'' = 1$ mechanism onset of 750 ± 100 K in both air and N_2.

The large-scale wind-tunnel application database for quantitative LRS now includes a subsonic–transonic cryogenic high-pressure nitrogen facility, a Mach 22 helium facility, a Mach 6 air facility with $T_0 = 700$ K, and a Mach 10 air facility with $T_0 = 990$ K. When the $V'' = 1$ mechanism is active, LRS can be used for quantitative density measurements at densities that are well below the liquid-vapor saturation curve, span the supersaturated region, and intersect the condensation onset region. For both the 20M6 and 15M6 air facilities with T_1 spanning 58–85 K when no $V'' = 1$ mechanism is present, results indicate molecular scattering will be observed when freestream pressures are two orders of magnitude below the liquid-vapor curve. These results provide guidance when considering LRS as a quantitative diagnostic for hypersonic wind tunnels.

Since their inception in the 1940s, progress in constructing increasingly higher Mach number hypersonic wind tunnels has been hampered by clustering and condensation. By removing water, adding filters to decrease particulates, using nitrogen to avoid the condensable components in air and, finally, materials to withstand the high stagnation reservoir temperatures, Mach numbers of 18–22 have been attained. Results in air in this study and nitrogen in previous AEDC T9 studies indicate the energy frozen in vibrational populations can improve flow quality, prevent clustering, and delay condensation onset beyond the well-known curves of Daum and Gyarmathy [16]. This mechanism could significantly impact the design and use of hypersonic facilities by making it possible to operate beyond the supersaturated/supercooled region to enlarge the Mach-Reynolds number test envelope. If some economical non-thermal method could be found to produce significant vibrational populations in the stagnation chamber, hypersonic facilities could be operated cluster free and possibly condensation free at lower stagnation temperatures. It was suggested that this can be accomplished using non-self-sustained discharges [41]. A discharge will change the state of matter from a gas to a plasma. In air, this will produce minor species such as O_3, NO, and NO_2 in the stagnation chamber along with N_2O_4 by recombination of NO_2 during the expansion process. It would be interesting to study whether the increase in vibrational population overcomes the enhanced clustering these species are likely to create. In pure nitrogen, assuming complete plasma recombination to a gas before the test section, this may be a useful approach. In a general sense, these statements are true for any long-lived chemically nonreactive energetic substance. The authors suggest another possibility is the introduction of high-electronic-energy long-lived metastable species, such as krypton ($4p^5 5s^2[\frac{3}{2}]_2$ state), argon ($3p^5 4s^2[\frac{3}{2}]_2$ state), and

$$N_2\left(A^3 \sum_u^+ \text{state}\right)$$

Argon-fluoride excimer-laser production of metastable krypton has been discussed [42]. Future research to explore all these possibilities is anticipated.

To further support the conclusions of this and future studies, new instrumentation is vital. It should be capable of at least measuring the freestream vibrational nonequilibrium Boltzmann population and, if possible, in situ measurements of cluster composition, cluster size distributions, kinetics, and growth mechanisms. After 70 years of study, this would provide at least some hope of eventually understanding the subtleties of clustering and condensation in hypersonic and hypervelocity facilities.

Acknowledgments

The successful and timely completion of the experiments would have been difficult without Mark Kulick providing the expert mechanical design and assembly of structures to support the laser, camera, and optics. In-depth discussions of the facility calibrations and processes with Matt Rhode of the Aerothermodynamics Branch are gratefully acknowledged. The contributions of Andrew McCrea are recognized for providing the virtual diagnostics renderings. We thank the anonymous referees for comments that improved the paper. The use of trademarks or names of manufacturers in this paper is for accurate reporting and does not constitute an official endorsement, either expressed or implied, of such products or manufacturers by the NASA.

References

[1] Miles, R. B., Lempert, W. R., and Forkey, J. N., "Laser Rayleigh Scattering," *Measurement Science and Technology*, Vol. 12, No. 5, 2001, pp. R33–R51. doi:10.1088/0957-0233/12/5/201

[2] Dyer, T. M., "Rayleigh Scattering Measurements of Time-Resolved Concentration in a Turbulent Propane Jet," *AIAA Journal*, Vol. 17, No. 8, 1979, pp. 912–914. doi:10.2514/3.61247

[3] Escoda, M. C., and Long, M. B., "Rayleigh Scattering Measurements of the Gas Concentration Field in Turbulent Jets," *AIAA Journal*, Vol. 21, No. 1, 1983, pp. 81–84. doi:10.2514/3.8031

[4] Yip, B., Fourguette, D. C., and Long, M. B., "Three- Dimensional Gas Concentration and Gradient Measurements in a Photo-acoustically Perturbed Jet," *Applied Optics*, Vol. 25, No. 21, 1986, pp. 3919–3923. doi:10.1364/AO.25.003919

[5] Grunefeld, G., Beushausen, V., and Andresen, P., "Planar Air Density Measurements near Model Surfaces by Ultraviolet Rayleigh/Raman Scattering," *AIAA Journal*, Vol. 32, No. 7, 1994, pp. 1457–1463. doi:10.2514/3.12216

[6] Dam, N. J., Rodenburg, M., Tolboom, R. A. L., Stoffels, G. G. M., Huisman-Kleinherenbrink, P. M., and ter Meulen, J. J., "Imaging of an Underexpanded Nozzle Flow by UV Laser Rayleigh Scattering," *Experiments in Fluids*, Vol. 24, 1998, pp. 93–101. doi:10.1007/s003480050156

[7] Fourguette, D. C., Mungal, M. G., and Dibble, R. W., "Time Evolution of the shear Layer of a Supersonic Axisymmetric Jet," *AIAA Journal*, Vol. 29, No. 7, 1991, pp. 1123–1130. doi:10.2514/3.10712

[8] Smith, M., Smits, A., and Miles, R., "Compressible Boundary-Layer Density Cross Sections by UV Rayleigh Scattering," *Optics Letters*, Vol. 14, 1989, pp. 916–918. doi:10.1364/OL.14.000916

[9] Shirinzadeh, B., Hillard, M. E., and Exton, R. J., "Condensation Effects on Rayleigh Scattering Measurements in a Supersonic Wind Tunnel," *AIAA Journal*, Vol. 29, No. 2, Feb. 1991, pp. 242–246. doi:10.2514/3.10570

[10] Shirinzadeh, B., Hillard, M. E., Balla, R. J., Waitz, I. A., Anders, J. B., and Exton, R. J., "Planar Rayleigh Scattering Results in Helium-Air Mixing Experiments in a Mach-6 Wind Tunnel," *Applied Optics*, Vol. 31, 1992, pp. 6529–6534. doi:10.1364/AO.31.006529

[11] Shirinzadeh, B., Balla, R. J., and Hillard, M. E., "Rayleigh Scattering Measurements in Supersonic Facilities," AIAA Paper 1996-2187, June 1996.

[12] Wu, P., Lempert, W. R., and Miles, R. B., "MHz Pulse-Burst Laser System and Visualization of Shock-Wave Boundary-Layer Interaction in a Mach 2.5 Wind Tunnel," *AIAA Journal*, Vol. 38, No. 4, 2000, pp. 672–679. doi:10.2514/2.1009

[13] Hansen, F. C., and Nothwang, G. J., "Condensation of Air in Supersonic Wind Tunnels and its Effects on Flow About Models," NACA TN 2690, April 1952.

[14] Becker, J. V., "Results of Recent Hypersonic and Unsteady Flow Research at the Langley Aeronautical Laboratory," *Journal of Applied Physics*, Vol. 21, No. 7, 1950, pp. 619–628. doi:10.1063/1.1699720

[15] Daum, F. L., "Air Condensation in a Hypersonic Wind Tunnel," *AIAA Journal*, Vol. 1, No. 5, 1963, pp. 1043–1046. doi:10.2514/3.1722

[16] Daum, F. L., and Gyarmathy, G., "Condensation of Air and Nitrogen in Hypersonic Wind Tunnels," *AIAA Journal*, Vol. 6, No. 3, 1968, pp. 458–465. doi:10.2514/3.4520

[17] Willmarth, W. W., and Nagamatsu, H. T., "The Condensation of Nitrogen in a Hypersonic Tunnel," *Journal of Applied Physics*, Vol. 23, No. 10, 1952, pp. 1089–1095. doi:10.1063/1.1701991

[18] Shirinzadeh, B., Herring, G. C., and Barros, T., "Demonstration of Imaging Flow Diagnostics Using Rayleigh Scattering in Langley 0.3-Meter Transonic Cryogenic Tunnel," NASA TM-1999-208970, 1999.

[19] Herring, G. C., Hillard, Jr., and Melvin, E., "Flow Visualization by Elastic Light Scattering in the Boundary Layer of a Supersonic Flow," NASA TM-2000-210121, 2000.

[20] Hoppe, J. C., and Honaker, W. C., "The Application of Laser Rayleigh Scattering to Gas Density Measurements in Hypersonic Helium Flows," AIAA Paper 1979-1086, June 1979.

[21] Micol, J. R., "Langley Aerothermodynamic Facilities Complex: Enhancements and Testing Capabilities," AIAA Paper 1998-0147, 1998.

[22] Bohren, C. F., and Huffman, D. R., *Absorption and Scattering of Light by Small Particles*, Wiley-Interscience, New York, 1983, p. 130.

[23] Bates, D. R., "Rayleigh Scattering by Air," *Planetary and Space Science*, Vol. 32, 1984, pp. 785–790. doi:10.1016/0032-0633(84)90102-8

[24] Bucholtz, A., "Rayleigh-Scattering Calculations for the Terrestrial Atmosphere," *Applied Optics*, Vol. 34, 1995, pp. 2765–2773. doi:10.1364/AO.34.002765

[25] Karlsson, B., and Ribbing, C. G., "Optical Constants and Spectral Selectivity of Stainless Steel and its Oxides," *Journal of Applied Physics*, Vol. 53, No. 9, 1982, pp. 6340–6346. doi:10.1063/1.331503

[26] Hollis, B. R., "Real-Gas Flow Properties for NASA Langley Research Center Aerothermodynamic Facilities Complex Wind Tunnels," NASA CR 4755, Sept. 1996.

[27] Schwartz, R. J., "ViDi: Virtual Diagnostics Interface Volume 1: The Future of Wind Tunnel Testing," NASA CR-2004-212667, Jan. 2004.

[28] Furukawa, G. T., and McCoskey, R. E., "The Condensation Line of Air and the Heats of Vaporization of Oxygen and Nitrogen," NACA TN 2969, June 1953.

[29] Wegener, P. P., "Nucleation of Nitrogen: Experiment and Theory," *Journal of Physical Chemistry*, Vol. 91, 1987, pp. 2479–2481. doi:10.1021/j100294a007

[30] Pal, P., and Hoare, M. R., "Thermodynamics Properties and Homogeneous Nucleation of Molecular Clusters of Nitrogen," *Journal of Physical Chemistry*, Vol. 91, 1987, pp. 2474–2479. doi:10.1021/j100294a006

[31] Wagner, P. E., "Condensation Processes in Aerosols," *Journal of Aerosol Science*, Vol. 26, No. 1, 1995, pp. S203–S204. doi:10.1016/0021-8502(95)97009-4

[32] Bae, H., Kim, I., Kim, E., and Lee, J., "Generation of Nano-Sized Ar-N2 Compound Particles by Homogeneous Nucleation and Heterogenous Growth in a Supersonic Expansion," *Journal of Aerosol Science*, Vol. 41, 2010, pp. 243–256. doi:10.1016/j.jaerosci.2009.11.005

[33] Wagner, P. E., "Homogeneous and Heterogeneous Nucleation in Multicomponent Systems," *Journal of Aerosol Science*, Vol. 35, No. S2, 2004, pp. 783–784. doi:10.1016/j.jaerosci.2004.06.007

[34] Stauffer, D., Kiang, C. S., Eggington, A., Patterson, E. M., Puri, O. P., Walker, G. H., and Wise, J. D., "Heterogeneous Nucleation and Fisher's Droplet Picture," *Physical Review B*, Vol. 6, 1972, pp. 2780–2783. doi:10.1103/PhysRevB.6.2780

[35] Anderson, J. D., *Hypersonic and High Temperature Gas Dynamics*, 1st ed., McGraw–Hill, New York, 1989, pp. 482–491.

[36] Griffith, W. C., Yanta, W. J., and Ragsdale, W. C., "Supercooling in Hypersonic Nitrogen Wind Tunnels," *Journal of Fluid Mechanics*, Vol. 269, 1994, pp. 283–299. doi:10.1017/S0022112094001564

[37] Marren, D. E., and Lafferty, J. F., "Experimental Determination of the Limits of Supercooling in the Hypervelocity Wind Tunnel No. 9," AIAA Paper 1994-0199, Jan. 1994.

[38] Lederer, M., Yanta, W., Ragsdale, W., Hudson, S., and Griffith, W., "Condensation in Hypersonic Nitrogen Tunnels," AIAA Paper 1990-1392, 1990.

[39] Dolgushev, S. V., Drucker, I. G., Korobeinikov, Y. G., Sapogov, B. A., and Safronov, Y. A., "Nitrogen Condensation in a Hypersonic Nozzle," *Journal of Engineering Physics and Thermophysics*, Vol. 49, 1985, pp. 899–902.

doi:10.1007/BF00872639
[40] Rich, J. W., "Relaxation of Molecules Exchanging Vibrational Energy," *Applied Atomic Collision Physics*, edited by E. W. McDaniel, and W. L. Nighan, Vol. 3, Academic Press, New York 1982, Chap. 4.
[41] Montello, A., Nishihara, M., Rich, J. W., Adamovich, I. V., and Lempert, W. R., "Picosecond CARS Measurements of Vibrational Distribution Functions in a Nonequilibrium Mach 5 Flow," AIAA Paper 2011-1322, 2011.
[42] Mills, J. L., Sukenik, C. I., and Balla, R. J., "Hypersonic Wake Diagnostics Using Laser Induced Fluorescence Techniques," AIAA Paper 2011-3459, 2011.

F. Alvi
Associate Editor